Mathematical Structure of Modal Interactions in a Spinning Disk-Stationary Load System

Jen-San Chen
Graduate Student.

D. B. Bogy
Professor,
Mem. ASME.

Department of Mechanical Engineering,
Computer Mechanics Laboratory,
University of California,
Berkeley, CA 94720

In a previous paper (Chen and Bogy, 1992) we studied the effects of various load parameters, such as friction force, transverse mass, damping, stiffness and the analogous pitching parameters, of a stationary load system in contact with the spinning disk on the natural frequencies and stability of the system when the original eigenvalues of interest are well separated. This paper is a follow-up investigation to deal with the situations in which two eigenvalues of the freely spinning disk are almost equal (degenerate) and strong modal interactions occur when the load parameters are introduced. After comparing an eigenfunction expansion with the finite element numerical results, we find that for each of the transverse and pitching load parameters, a properly chosen two-mode approximation can exhibit all the important features of the eigenvalue changes. Based on this two-mode approximation we study the mathematical structure of the eigenvalues in the neighborhood of degenerate points in the natural frequency-rotation speed plane. In the case of friction force, however, it is found that at least a four-mode approximation is required to reproduce the eigenvalue structure. The observations and analyses presented provide physical insight into the modal interactions induced by various load parameters in a spinning disk-stationary load system.

Introduction

The dynamics of a spinning disk in contact with a stationary load system has attracted much attention because of its applications in such fields as computer disk memory units and circular saws. Iwan and Moeller's (1976) work appears to be the first publication on this subject in which they calculated the natural frequencies of vibration and discussed the instabilities caused by the addition of translational mass, damping, and stiffness in the load system. Ono et al. (1991) extended Iwan and Moeller's work to include the corresponding rotational (pitching) parameters in the load system as well as the friction force between the spinning disk and the stationary load system (see Fig. 1). They concluded that pitching parameters have similar effects as their transverse counterparts and friction force tends to destabilize the forward travelling wave but stabilizes the reflected and backward travelling waves. In an attempt to give an explanation of these phenomena observed from calculations, Chen and Bogy (1992) derived expressions for the derivatives of the eigenvalues with respect to various parameters in the load system. However, this formulation is useful only when the eigenvalues of interest are well separated and interactions between the neighboring modes are negligible. However, it is not uncommon that some eigenvalues (which are purely imaginary in the case of a freely spinning disk) are

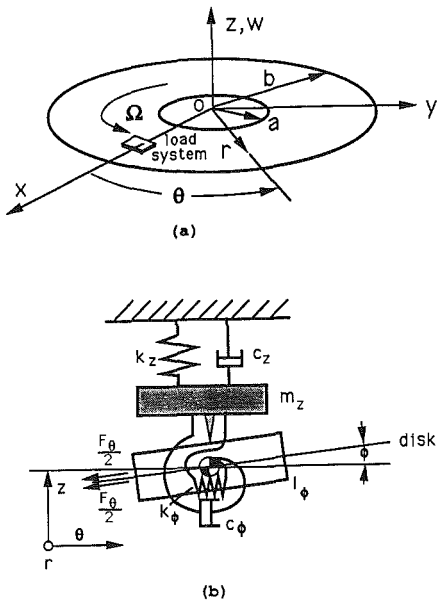

Fig. 1(*a*) Global picture of the spinning disk and the stationary load system, (*b*) parameters in the load system

Contributed by the Applied Mechanics Division of THE AMERICAN SOCIETY OF MECHANICAL ENGINEERS for presentation at the 1992 ASME Summer Mechanics and Materials Meeting, Tempe, AZ, Apr. 28–May 1, 1992.

Discussion on this paper should be addressed to the Technical Editor, Professor Leon M. Keer, The Technological Institute, Northwestern University, Evanston, IL 60208, and will be accepted until four months after final publication of the paper itself in the JOURNAL OF APPLIED MECHANICS. Manuscript received by the ASME Applied Mechanics Division, Apr. 10, 1991; final revision, July 11, 1991.

Paper No. 92-APM-20.

Copyright © 1992 by ASME
Downloaded 16 Oct 2008 to 140.112.113.225. Redistribution subject to ASME license or copyright; see http://www.asme.org/terms/Terms_Use.cfm

very close to each other, or even identical. In such cases, the strong interactions between the neighboring modes have to be taken into account when the load parameters are applied. Although modal interactions in a spinning disk-stationary load system have been recognized for some time, the mathematical structure of these phenomena was not well understood.

While perturbation theory is a useful approach for dealing with this problem (Perkins and Mote, 1986), it encounters the difficulty that the radius of convergence of the perturbation series may approach zero as the unperturbed eigenvalues in question get closer to each other. In particular, when two eigenvalues coincide, the radius of convergence may vanish and the perturbation problem becomes singular (Bender and Orszag, 1978).

In the present paper we study the mathematical structure of this eigenvalue problem when two eigenvalues are identical or very close to each other in the frequency-rotation speed parameter space. By using the orthogonality relations developed in Chen and Bogy (1992) and the eigenfunction expansion method, we replace the original partial differential equation by a system of infinite linear homogeneous algebraic equations. Through a sequence of approximations obtained by truncating an infinite dimensional matrix, we establish that the sequence converges very fast to the exact solution in the presence of both the transverse and pitching parameters. Furthermore, it is found that a simple two-mode approximation displays the general features of the eigenvalue changes with the load parameters. Based on the two-mode approximation, we examine analytically the properties of the perturbed eigenvalues as functions of the load parameters when two modes are almost degenerate.

Equation of Motion

Consider a circular, elastic disk rotating in contact with a stationary load system containing transverse mass m_z, spring k_z, dashpot c_z, and the analogous pitching elements I_ϕ, k_ϕ, c_ϕ, as shown in Fig. 1. In addition, the load system applies a constant friction force F_θ to the disk in the circumferential direction at the coupling point between the load system and the spinning disk. The equation of motion of this coupled system, in terms of transverse displacement w and with respect to the stationary coordinate system (r, θ), can be written as

$$\rho h(w_{,tt}+2\Omega w_{,t\theta}+\Omega^2 w_{,\theta\theta})+D\nabla^4 w-\frac{h}{r}(\sigma_r r w_{,r})_{,r}-\frac{h\sigma_\theta}{r^2}w_{,\theta\theta}$$
$$=-\frac{1}{r}\delta(r-\xi)\delta(\theta)\left(m_z w_{,tt}+c_z w_{,t}+k_z w+\frac{F_\theta}{r}w_{,\theta}\right)$$
$$+\frac{1}{r^3}\delta(r-\xi)[(I_\phi w_{,tt\theta}+c_\phi w_{,t\theta}+k_\phi w_{,\theta})\delta(\theta)]_{,\theta} \quad (1)$$

where

$$D=\frac{Eh^3}{12(1-\nu^2)}, \quad \nabla^4=\left(\frac{\partial^2}{\partial r^2}+\frac{1}{r}\frac{\partial}{\partial r}+\frac{1}{r^2}\frac{\partial^2}{\partial\theta^2}\right)^2.$$

The parameters Ω, ρ, h, E, and ν are the rotation speed, density, thickness, Young's modulus, and Poisson's ratio of the disk. $\delta(:)$ is the Dirac delta function. The coupling position between the load system and disk is assumed to be $r = \xi$ and $\theta = 0$. The spinning disk is clamped at the inner radius $r = a$ and free at the outer radius $r = b$. The generalized plane stresses σ_r and σ_θ are due to the centrifugal effect. We neglect the effect of the friction force on these in-plane stresses because the coefficients of friction in the systems of interest are usually relatively low. Equation (1) can be rewritten in the operator form

$$(M+\hat{M})w_{,tt}+(G+\hat{G})w_{,t}+(K+\hat{K})w=0 \quad (2)$$

where

$$M=\rho h$$

$$\hat{M}=\delta(r-\xi)\delta(\theta)\left(\frac{m_z}{r}-\frac{I_\phi}{r^3}\frac{\partial^2}{\partial\theta^2}\right)-\frac{I_\phi}{r^3}\delta(r-\xi)\delta'(\theta)\frac{\partial}{\partial\theta}$$

$$G=2\rho h\Omega\frac{\partial}{\partial\theta}$$

$$\hat{G}=\delta(r-\xi)\delta(\theta)\left(\frac{c_z}{r}-\frac{c_\phi}{r^3}\frac{\partial^2}{\partial\theta^2}\right)-\frac{c_\phi}{r^3}\delta(r-\xi)\delta'(\theta)\frac{\partial}{\partial\theta}$$

$$K=D\nabla^4+\rho h\left[\Omega^2\frac{\partial^2}{\partial\theta^2}-\frac{1}{\rho r}\frac{\partial}{\partial r}\left(\sigma_r r\frac{\partial}{\partial r}\right)-\frac{\sigma_\theta}{\rho r^2}\frac{\partial^2}{\partial\theta^2}\right]$$

$$\hat{K}=\delta(r-\xi)\delta(\theta)\left(\frac{k_z}{r}-\frac{k_\phi}{r^3}\frac{\partial^2}{\partial\theta^2}+\frac{F_\theta}{r^2}\frac{\partial}{\partial\theta}\right)$$
$$-\frac{k_\phi}{r^3}\delta(r-\xi)\delta'(\theta)\frac{\partial}{\partial\theta}.$$

$\delta'(:)$ is the derivative of the Dirac delta function.

Equation (2) can also be cast in the first-order operator form

$$(\mathbf{A}+\hat{\mathbf{A}})\mathbf{x}_{,t}-(\mathbf{B}+\hat{\mathbf{B}})\mathbf{x}=\mathbf{0} \quad (3)$$

by defining the state vector

$$\mathbf{x}\equiv\begin{Bmatrix} w_{,t} \\ w \end{Bmatrix}$$

and the matrix differential operators

$$\mathbf{A}\equiv\begin{bmatrix} M & 0 \\ 0 & K \end{bmatrix}, \quad \hat{\mathbf{A}}\equiv\begin{bmatrix} \hat{M} & 0 \\ 0 & \hat{K} \end{bmatrix},$$

$$\mathbf{B}\equiv\begin{bmatrix} -G & -K \\ K & 0 \end{bmatrix}, \quad \hat{\mathbf{B}}\equiv\begin{bmatrix} -\hat{G} & -\hat{K} \\ \hat{K} & 0 \end{bmatrix}.$$

For a freely spinning disk (i.e., in the absence of the load system), Eq. (2) can be reduced to

$$Mw_{,tt}+Gw_{,t}+Kw=0. \quad (4)$$

Since M and K are symmetric and G is skew, Eq. (4) is a standard gyroscopic equation. The eigenvalues of the $e^{\lambda t}$ time-reduced form of Eq. (4), together with the associated homogeneous boundary conditions, are purely imaginary and occur in complex conjugate pairs, i.e., $\lambda^0_{mn} = i\omega_{mn}$, where ω_{mn} is real. The eigenfunction corresponding to λ^0_{mn} is in general complex and assumes the form

$$w^0_{mn}=R_{mn}(r)e^{\pm in\theta}. \quad (5)$$

R_{mn} is a real-valued function of r. The eigenfunction corresponding to $\bar{\lambda}^0_{mn}$ is $\bar{w}^0_{mn}$, where overbar means complex conjugate. If we consider only the positive ω_{mn}, then w^0_{mn} in Eq. (5) with $+in\theta$ is a backward travelling wave with n nodal diameters and m nodal circles, which is also denoted by $(m, n)_b$. Similarly, w^0_{mn} with $-in\theta$ is a forward travelling wave $(m, n)_f$. Of interest is the dependence of the natural frequencies on the rotation speed Ω. The critical speed Ω_c for the mode (m, n) is defined as the rotation speed at which ω_{mn} of the backward travelling wave $(m, n)_b$ is zero. For Ω greater than Ω_c, this mode is a forward travelling wave, and is called a "reflected wave," denoted by $(m, n)_r$. Figure 2 shows the natural frequencies, both positive and negative, for a 5.25-in. computer floppy disk as functions of rotation speed. This result is obtained from a finite element computation presented in Ono et al. (1991). The material properties of the disk used in the calculation are $\rho = 1.3 \times 10^3$ kg/m^3, $E = 4.9 \times 10^9$ N/m^2, $\nu = 0.3$, $h = 0.078$ mm, $a = 17.5$ mm, $b = 65.0$ mm, and $\xi/b = 0.75$.

It is noted from Fig. 2 that there are four different situations in which two eigenvalues become degenerate, that is, the natural frequency loci intersect.

Case A: A reflected wave meets a backward wave, for example, point A is the intersection of modes $(0,2)_r$ and $(0,1)_b$.

Downloaded 16 Oct 2008 to 140.112.113.225. Redistribution subject to ASME license or copyright; see http://www.asme.org/terms/Terms_Use.cfm

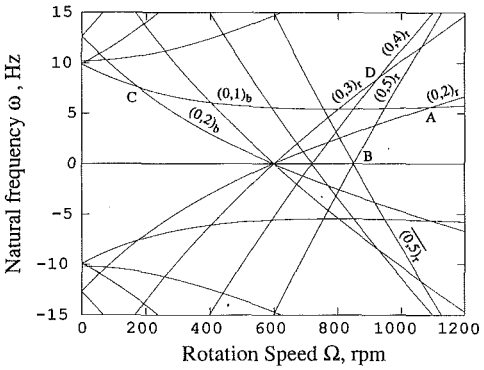

Fig. 2 Natural frequency versus rotation speed for a freely spinning disk

Case B: A backward wave meets its complex conjugate at its critical speed, for example, point B is the intersection of mode (0,5) and its complex conjugate, $(\overline{0,5})$.

Case C: A forward or backward wave meets another forward or backward wave, for example, point C is the intersection of modes $(0,2)_b$ and $(0,1)_b$.

Case D: A reflected wave meets another reflected wave, for example, point D is the intersection of modes $(0,3)_r$ and $(0,4)_r$.

In the following, we shall study the behavior of eigenvalue changes in the neighborhood of these intersection points resulting from the addition of various load parameters.

Orthogonality Relations and Eigenfunction Expansion Theorem

It has been shown in Chen and Bogy (1992) that for a freely spinning disk, the orthogonality relations among the eigenfunctions can be written as follows:

$$\langle \mathbf{x}^0_{mn},\ \mathbf{A}\mathbf{x}^0_{pq}\rangle = 0,\ \langle \mathbf{x}^0_{mn}, \mathbf{B}\mathbf{x}^0_{pq}\rangle = 0 \quad \text{if } \lambda^0_{mn} \neq \lambda^0_{pq} \tag{6}$$

where the inner product between two vectors $\mathbf{x}_{mn}$ and $\mathbf{x}_{pq}$ is defined as

$$\langle \mathbf{x}_{mn}, \mathbf{x}_{pq}\rangle = \int_0^{2\pi}\int_a^b \bar{\mathbf{x}}^T_{mn}\mathbf{x}_{pq} r dr d\theta$$

and $\mathbf{x}^T_{mn}$ is the transpose of the state vector $\mathbf{x}_{mn}$. In addition,

$$\lambda^0_{mn} = \frac{\langle \mathbf{x}^0_{mn}, \mathbf{B}\mathbf{x}^0_{mn}\rangle}{\langle \mathbf{x}^0_{mn}, \mathbf{A}\mathbf{x}^0_{mn}\rangle}. \tag{7}$$

To obtain the eigenvalues of Eq. (2) or (3) for the disk-load system, we represent its eigenfunction solution as an expansion in terms of the eigenfunctions of the freely spinning disk. Before proceeding further, it is desirable to argue that the eigenfunction expansion theorem holds in this case, i.e., every continuous complex function $f(r,\theta)$ satisfying the prescribed boundary conditions can be expanded in a uniformly convergent series in the eigenfunctions of the unloaded system

$$f(r,\theta) = \sum_{m=0}^{\infty}\sum_{n=-\infty}^{\infty} c_{mn} w^0_{mn}(r,\theta).$$

First we observe that the complex functions $\{e^{\pm in\theta}\}$ are complete, in the L_2 sense, in the domain $(0, 2\pi)$. By substituting the separable solution

$$w_{mn}(r,\theta,t) = R_{mn}(r) e^{i(\omega_{mn} t \pm n\theta)}$$

into Eq. (4) we get, for each n, an ordinary differential equation for $R_{mn}(r)$,

$$Q_n R_{mn}(r) = (\omega_{mn} \pm n\Omega)^2 R_{mn}(r)$$

where

$$Q_n = \frac{D}{\rho h}\left(\frac{\partial^2}{\partial r^2} + \frac{\partial}{r\partial r} - \frac{n^2}{r^2}\right)^2 - \left[\frac{\partial}{\rho r \partial r}\left(\sigma_r r \frac{\partial}{\partial r}\right) - \frac{n^2\sigma_\theta}{\rho r^2}\right].$$

Since Q_n is a self-adjoint linear differential operator in the domain $a \le r \le b$, the system of eigenfunctions $R_{mn}(r)$ is complete (Stakgold, 1979), in the L_2 sense, and the expansion theorem holds for $R_{mn}(r)$. Through a standard procedure for constructing a complete system of functions of two variables (Courant and Hilbert, 1962), it is established that the functions $\{R_{mn}(r)e^{\pm in\theta}\}$ form a complete system of functions in r and θ in the domain $0 < \theta \le 2\pi$, $a \le r \le b$.

After establishing the completeness of the eigenfunctions for a freely spinning disk, we can expand the eigenfunction solution $\mathbf{x}$ of Eq. (3) as the infinite linear combination

$$\mathbf{x} = \sum_{p=0}^{\infty}\sum_{q=-\infty}^{\infty} c_{pq}\mathbf{x}^0_{pq} \tag{8}$$

Substituting Eq. (8) into (3) and taking the inner product between $\mathbf{x}^0_{mn}$ and both sides of Eq. (3), with use of the orthogonality properties (6) and Eq. (7) we get

$$c_{mn}(\lambda - \lambda^0_{mn})\mathbf{A}^{mn}_{mn} + \sum_{p=0}^{\infty}\sum_{q=-\infty}^{\infty} c_{pq}(\lambda\hat{\mathbf{A}}^{mn}_{pq} - \hat{\mathbf{B}}^{mn}_{pq}) = 0$$

where

$$\mathbf{A}^{mn}_{pq} = \langle \mathbf{x}^0_{mn},\ \mathbf{A}\mathbf{x}^0_{pq}\rangle$$
$$\hat{\mathbf{A}}^{mn}_{pq} = \langle \mathbf{x}^0_{mn},\ \hat{\mathbf{A}}\mathbf{x}^0_{pq}\rangle$$
$$\hat{\mathbf{B}}^{mn}_{pq} = \langle \mathbf{x}^0_{mn},\ \hat{\mathbf{B}}\mathbf{x}^0_{pq}\rangle.$$

Continuing this procedure through all the eigenfunctions we obtain an infinite matrix equation satisfied by the coefficients c_{mn}:

$$\mathbf{H}\mathbf{c} = \mathbf{0}$$

where

$$\mathbf{H} = \begin{bmatrix} (\lambda-\lambda^0_{00})\mathbf{A}^{00}_{00} + \lambda\hat{\mathbf{A}}^{00}_{00} - \hat{\mathbf{B}}^{00}_{00} & \lambda\hat{\mathbf{A}}^{00}_{01} - \hat{\mathbf{B}}^{00}_{01} & \cdots \lambda\hat{\mathbf{A}}^{00}_{10} - \hat{\mathbf{B}}^{00}_{10} & \cdots \\ \lambda\hat{\mathbf{A}}^{01}_{00} - \hat{\mathbf{B}}^{01}_{00} & (\lambda-\lambda^0_{01})\mathbf{A}^{01}_{01} + \lambda\hat{\mathbf{A}}^{01}_{01} - \hat{\mathbf{B}}^{01}_{01} & \cdots \lambda\hat{\mathbf{A}}^{01}_{10} - \hat{\mathbf{B}}^{01}_{10} & \cdots \\ \vdots & \vdots & & \\ \lambda\hat{\mathbf{A}}^{10}_{00} - \hat{\mathbf{B}}^{10}_{00} & \lambda\hat{\mathbf{A}}^{10}_{01} - \hat{\mathbf{B}}^{10}_{01} & & \vdots \\ \vdots & \vdots & & \end{bmatrix}$$

and

$$\mathbf{c} = (c_{00},\ c_{01},\ \cdots,\ c_{10},\ c_{11},\ \cdots)^T.$$

While in practice we are unable to deal with this infinite matrix $\mathbf{H}$, we can always devise an approximation sequence in which we expand $\mathbf{x}$ in terms of N modes with natural frequencies closest to the frequency range of interest. By doing so we can approximate Eq. (1) by a sequence of matrix equations

$$\mathbf{H}_N\mathbf{c}_N = \mathbf{0} \tag{9}$$

where the N by N matrix $\mathbf{H}_N$ is a truncation of matrix $\mathbf{H}$ by retaining only N rows and N columns. The existence of nontrivial solutions $\mathbf{c}_N$ satisfying Eq. (9) requires

$$\det\mathbf{H}_N = 0. \tag{10}$$

Equation (10) defines an Nth order polynomial in λ, which is a function of the various load parameters. In the following we will verify numerically the convergence of this approximation as N increases. It is noted that the off-diagonal terms in $\mathbf{H}_N$ are responsible for the modal interactions between these modes. In the special case in which only the diagonal terms

Downloaded 16 Oct 2008 to 140.112.113.225. Redistribution subject to ASME license or copyright; see http://www.asme.org/terms/Terms_Use.cfm

are retained, Eq. (10) is equivalent to a system of N uncoupled linear equations in λ, and the results can be reduced to those presented in Chen and Bogy (1992), where modal interactions were not considered.

Effects of Transverse Mass m_z

It has been shown in Chen and Bogy (1992) that the presence of m_z in the load system tends to decrease the natural frequencies of the forward and backward waves, but increases the natural frequencies of the reflected waves as long as the natural frequency of interest is well separated from the others. However, if two modes are almost degenerate, the modal interactions are so strong that these rules are no longer applicable. The dashed lines in Fig. 3(*a*) are the natural frequency loci of modes $(0, 2)_r$ and $(0, 1)_b$ for a freely spinning disk. These two modes are degenerate when the rotation speed, denoted by Ω_d, is 1092.1 rpm, which corresponds to point A in Fig. 2. The solid lines in Fig. 3(*a*) are the corresponding results for the case $m_z = 0.1\ g$. Both the solid and dashed lines are obtained by the finite element method. As m_z increases from zero and the rotation speed is lower than Ω_d, the natural frequencies tend to approach each other and eventually merge, while the real parts of λ_{mn} $(=\alpha_{mn} + i\omega_{mn})$ become nonzero and therefore instability is induced. On the other hand, no merging occurs when the rotation speed is higher than Ω_d. Moreover, when $\Omega = \Omega_d$ the natural frequencies separate, with one remaining unchanged and the other decreasing, as shown by the solid lines in Fig. 3(*a*). In Fig. 3(*b*) the rotation speed is fixed at 1090 rpm, just below Ω_d, while m_z ranges from 0 to 3g. The dashed lines, which are obtained by the finite element method show how the eigenvalues change as m_z increases. It is seen that these two natural frequency loci approach each other and merge for m_z greater than m_{z1}, and split again after m_z is greater than m_{z2}.

In order to reproduce the dashed lines in Fig. 3(*b*) by using the eigenfunction expansion method, we followed the procedure described in the preceding section. The solid lines in Fig. 3(*b*) show the progress of convergence as the number of eigenfunctions in the approximation increases. The eigenfunctions used in the expansion method are chosen in such a way

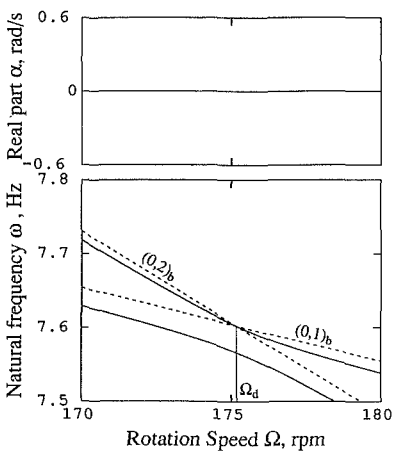

Fig. 4 Effects of transverse mass $m_z = 0.01g$ in case C. $\Omega_d = 175.5$ rpm.

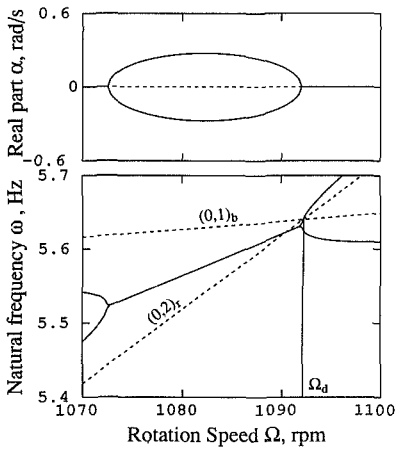

(*a*)

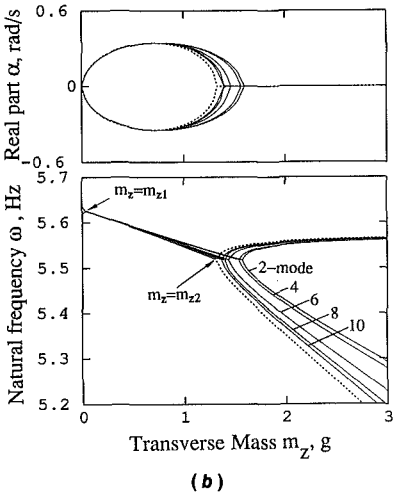

(*b*)

Fig. 3(*a*) Effects of transverse mass $m_z = 0.1g$ in case A. $\Omega_d = 1092.1$ rpm. (*b*) Eigenfunction expansion approximations at $\Omega = 1090$ rpm.

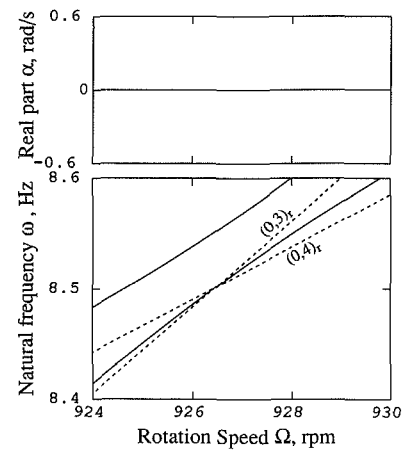

Fig. 5 Effects of transverse mass $m_z = 0.05g$ in case D

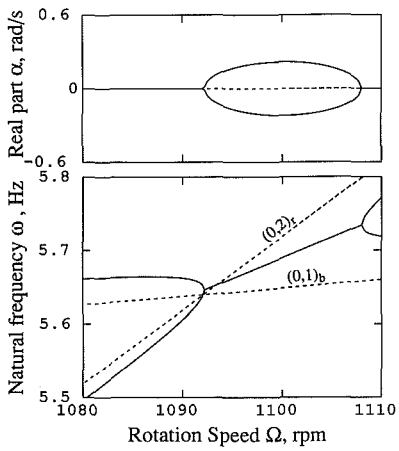

Fig. 6 Effects of transverse stiffness $k_z = 0.1$N/m in case A

Downloaded 16 Oct 2008 to 140.112.113.225. Redistribution subject to ASME license or copyright; see http://www.asme.org/terms/Terms_Use.cfm

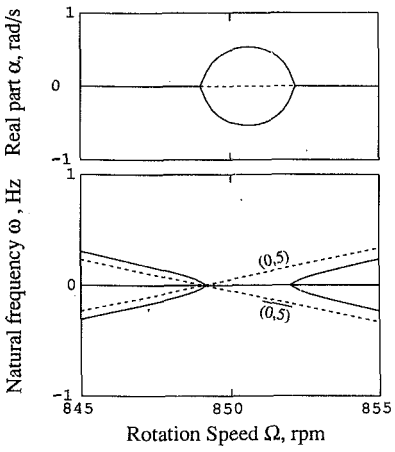

(a)

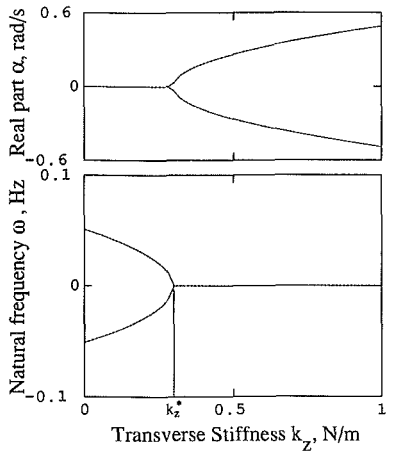

(b)

Fig. 7(*a*) Effects of transverse stiffness k_z = 1N/m in case B. Ω_c = 849.1 rpm. (*b*) Ω = 850 rpm.

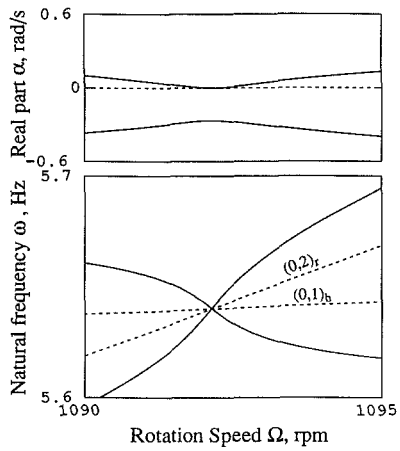

Fig. 8 Effects of transverse damping c_z = 0.01Ns/m in case A

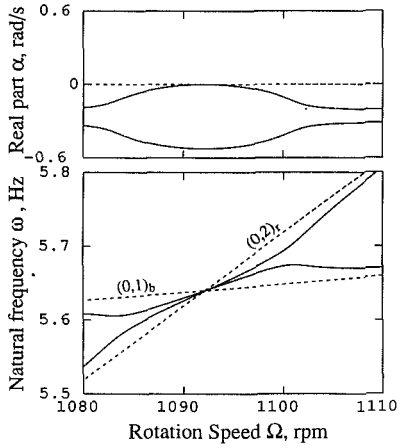

Fig. 9 Effects of friction force F_θ = 0.004N in case A

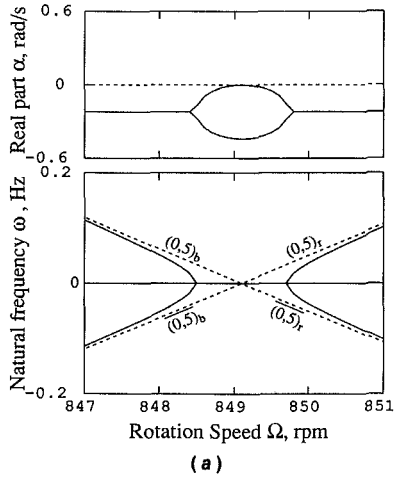

(a)

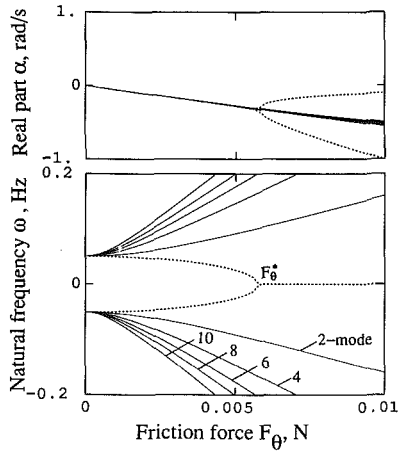

(b)

Fig. 10(*a*) Effects of friction force F_θ = 0.004N in case B. Ω_c = 849.1 rpm. (*b*) Eigenfunction expansion approximations at Ω = 850 rpm.

that their natural frequencies are closest to the frequency range of interest. It is found that the sequence of approximations converges monotonically to the finite element solution, the dashed lines. Furthermore, it is noted that even a simple two-mode approximation displays the important characteristics of the eigenvalue changes, i.e., the existence of a region between m_{z1} and m_{z2} in which two neighboring natural frequency loci merge and one of the modes becomes unstable.

The results presented in Fig. 4 through Figs. 10 are obtained by the finite element method, except those in Figs. 7(*b*) and 10(*b*). The dashed lines in Fig. 4 are the natural frequency loci of modes $(0,2)_b$ and $(0,1)_b$ for the freely spinning disk. These two modes are degenerate at Ω_d = 175.5 rpm, corresponding to point C in Fig. 2. The solid lines correspond to the case of m_z = 0.01 g. It is seen that these two loci veer away from each other in the ω–Ω plane and the degenerate natural frequencies separate with one remaining unchanged at point C and the other decreasing. No instability occurs in this case, since the real part of λ_{mn} remains zero.

Figure 5 shows the effect of m_z on the natural frequencies in the neighborhood of the intersection of two reflected waves $(0,3)_r$ and $(0,4)_r$, corresponding to point D in Fig. 2. The solid

Downloaded 16 Oct 2008 to 140.112.113.225. Redistribution subject to ASME license or copyright; see http://www.asme.org/terms/Terms_Use.cfm

lines correspond to the case of $m_z = 0.05$ g, and it is seen that mass causes these two loci to veer away from each other, as in the case of two backward waves, point C.

In the neighborhood of the intersection of a backward wave and its complex conjugate pair, as for point B in Fig. 2, it is found that m_z has very little effect on the natural frequencies, and no instability is induced.

In order to understand the mathematical structure of these phenomena, we look into the details of the two-mode approximation. Assume for the freely spinning disk that the two neighboring modes of interests are w^0_{mn} and w^0_{pq} with natural frequencies ω_{mn} and ω_{pq}, respectively,

$$w^0_{mn} = R_{mn}(r)e^{in\theta}$$
$$w^0_{pq} = R_{pq}(r)e^{iq\theta}.$$

For convenience, we define some constants

$$R^*_{mn} = \int_a^b R^2_{mn}(r)rdr, \qquad R^*_{pq} = \int_a^b R^2_{pq}(r)rdr$$

$$S_{mn} = R^*_{mn}(\omega_{mn} + n\Omega)R^2_{pq}(\xi), \qquad S_{pq} = R^*_{pq}(\omega_{pq} + q\Omega)R^2_{mn}(\xi)$$

which will be used throughout. For this two-mode approximation, Eq. (10) now becomes a quadratic equation in the eigenvalue λ,

$$(\alpha_0 + \alpha_1\epsilon)\lambda^2 + (\beta_0 + \beta_1\epsilon)\lambda + \gamma_0 = 0 \tag{11}$$

where

$$\left.\begin{aligned}
\alpha_0 &= 16\pi^2\omega_{mn}\omega_{pq}(\omega_{mn} + n\Omega)(\omega_{pq} + q\Omega)R^*_{mn}R^*_{pq}\\
\alpha_1 &= 4\pi\omega_{mn}\omega_{pq}\xi(\omega_{mn}S_{pq} + \omega_{pq}S_{mn})\\
\beta_0 &= -i(\omega_{mn} + \omega_{pq})\alpha_0\\
\beta_1 &= -4\pi i\omega^2_{mn}\omega^2_{pq}\xi(S_{mn} + S_{pq})\\
\gamma_0 &= -\omega_{mn}\omega_{pq}\alpha_0\\
\epsilon &= \frac{m_z}{\rho h\xi}
\end{aligned}\right\} \tag{12}$$

α_0, α_1, γ_0 are real and β_0 and β_1 are purely imaginary. The solution of (11) can be written in terms of the parameter ϵ as

$$\lambda_\pm = \frac{-(\beta_0 + \beta_1\epsilon) \pm [(\beta_0 + \beta_1\epsilon)^2 - 4\gamma_0(\alpha_0 + \alpha_1\epsilon)]^{1/2}}{2(\alpha_0 + \alpha_1\epsilon)} \tag{13}$$

This defines $\lambda_\pm(\epsilon)$, where ϵ must be real and positive. In order to understand the mathematical structure of λ, it is convenient to allow ϵ to be complex and consider $\lambda_\pm$ as functions of the complex variable ϵ, which are analytic except at the zeros of the square root term. The square root branch points of $\lambda_\pm(\epsilon)$ are

$$\epsilon_\pm = S_\pm(\omega_{pq} - \omega_{mn}) \tag{14}$$

where

$$S_\pm = \frac{4\pi S_{mn}S_{pq}}{(\sqrt{S_{mn}} \pm i\sqrt{S_{pq}})^2 R^2_{mn}(\xi)R^2_{pq}(\xi)\omega_{mn}\omega_{pq}\xi}.$$

In case A where w^0_{mn} is a backward wave and w^0_{pq} is a reflected wave, we have $n > 0$ and $q < 0$. According to Chen and Bogy (1992), it is found that $S_{mn} > 0$ and $S_{pq} < 0$. Therefore, $S_\pm$ are real and negative. When $\Omega < \Omega_d$, it follows that $\omega_{pq} < \omega_{mn}$, and consequently, the branch points $\epsilon_\pm$ are real and positive. We choose $|\epsilon_-| < |\epsilon_+|$. When ϵ is real and in the region (ϵ_-, ϵ_+), which corresponds to (m_{z1}, m_{z2}) in Fig. 3(*b*), the imaginary parts of the eigenvalues λ_- and λ_+ are identical and their real parts have opposite signs. When ϵ is real and outside the region (ϵ_-, ϵ_+), the real parts vanish and the imaginary parts are different. On the other hand, when $\Omega > \Omega_d$ the branch points are real and negative, and consequently no merging occurs. In the special case that $\Omega = \Omega_d$ and $\omega_{mn} = \omega_{pq} = \omega$, it is easy to verify that $\lambda = i\omega$ is a root of Eq. (11), and the other root is $\frac{i\alpha_0\omega}{\alpha_0 + \alpha_1\epsilon}$. This verifies the observation that one of the degenerate eigenvalues remains unchanged and the other changes. If the perturbed eigenvalue is written in the form of a power series in ϵ, as is the usual procedure in perturbation theory, it is obvious that the radius of convergence of the perturbation series is equal to $|\epsilon_-|$. From Eq. (14) it can be seen that this radius of convergence approaches zero as $\omega_{pq} - \omega_{mn}$ approaches zero. In particular, when $\omega_{mn} = \omega_{pq}$ the radius of convergence vanishes and the perturbation problem becomes singular.

In case C both w^0_{mn} and w^0_{pq} are backward waves, and $n > 0$, $q > 0$, $S_{mn} > 0$, $S_{pq} > 0$. As a result $S_\pm$ are complex conjugate pairs and so are $\epsilon_\pm$. Since the ϵ associated with the physical mass m_z is changed along the positive real line in the complex ϵ-plane and the branch points $\epsilon_\pm$ are complex, the square root term in Eq. (13) is always nonzero and purely imaginary. Consequently, λ_+ and λ_- remain purely imaginary and distinct and no frequency merging occurs. Again, at $\Omega = \Omega_d$ and $\omega_{mn} = \omega_{pq} = \omega$, the two eigenvalues are $i\omega$ and $\frac{i\alpha_0\omega}{\alpha_0 + \alpha_1\epsilon}$.

In case D, both w^0_{mn} and w^0_{pq} are reflected waves, and $n < 0$, $q < 0$, $S_{mn} < 0$, $S_{pq} < 0$. Again, $S_\pm$ are complex conjugate pairs and so are $\epsilon_\pm$. Therefore the conclusion in the preceding paragraph applies equally well to this case.

In the final case B, w_{mn} is a backward wave and w_{pq} is its complex conjugate, $w^0_{pq} = \overline{w}^0_{mn}$, and $\omega_{mn} = -\omega_{pq}$. β_0 and β_1 vanish and the eigenvalues are then readily obtained as

$$\lambda_\pm = \pm i\left[\frac{2\pi\omega^2_{mn}S_{mn}}{2\pi S_{mn} + \epsilon\omega_{mn}R^4_{mn}(\xi)\xi}\right]^{1/2}$$

where S_{mn} is positive. Apparently, $\lambda_\pm$ are purely imaginary and no instability is induced. Both of the degenerate eigenvalues with $\omega = 0$ remain zero, and the critical speed is not changed by m_z.

Effects of Transverse Stiffness k_z

In cases when the eigenvalue of interest is well separated from the others, k_z tends to increase the natural frequencies of the forward and backward waves but decrease the natural frequency of the reflected wave, just opposite to the effect of m_z. Similar to the case of m_z, these rules are not applicable when the eigenvalues are almost degenerate. Figure 6 shows the effect of $k_z = 0.1$N/m in the neighborhood where modes $(0,1)_b$ and $(0,2)_f$ are degenerate. When the rotation speed is higher than $\Omega_d = 1092.1$ rpm, these two natural frequency loci merge. On the other hand, no merging occurs when $\Omega < \Omega_d$. At Ω_d the degenerate eigenvalues separate, with one remaining unchanged and the other increasing. These phenomena are very similar to those for m_z, except that merging occurs on the opposite side of Ω_d. If we fix the rotation speed a little higher than Ω_d, say at 1094 rpm, and change k_z, we observe a region of k_z between k_{z1} and k_{z2}, in which two natural frequency loci merge and one of these two modes becomes unstable. This characteristic is very similar to that described in Fig. 3(*b*), in which m_z is present and the rotation speed is lower than Ω_d.

The effects of k_z in cases C and D are the same as those of m_z. Veering occurs in the ω-Ω diagram and no instability is induced, which is similar to the behaviors described in Figs. 4 and 5. These observations suggest that the mathematical structure for the effects of k_z and m_z are very similar in cases A, C, and D.

Around point B, which is the intersection of a backward wave and its complex conjugate pair, k_z changes the eigenvalues

Downloaded 16 Oct 2008 to 140.112.113.225. Redistribution subject to ASME license or copyright; see http://www.asme.org/terms/Terms_Use.cfm

in a unique way. Figure 7(*a*) shows that the natural frequency loci of modes (0,5) and $(\overline{0,5})$ merge and one of the modes becomes unstable when Ω is higher than the critical speed Ω_c = 849.1 rpm. When $\Omega < \Omega_c$ these loci tend to diverge away from each other and no instability is induced. In Fig. 7(*b*) the rotation speed is fixed at 850 rpm, a little higher than Ω_c, and k_z is changed from 0 to 1 N/m. The dashed and solid lines, obtained by finite element method and two-mode approximation, respectively, are almost indistinguishable. It is found that when k_z is increased to k_z^*, the natural frequency loci merge to the value zero. As k_z increases beyond k_z^*, the magnitude of the real part becomes larger. It is also confirmed, through additional calculations not shown here, that a two-mode expansion is a very good approximation to the finite element solution in the cases A, C, and D.

Analogous to the procedure used to study the effects of m_z, we next look into the details of the two-mode approximation for k_z. The eigenvalues $\lambda_\pm$ can be obtained by solving the following quadratic equation:

$$(\alpha_0+\alpha_1\epsilon)\lambda^2+(\beta_0+\beta_1\epsilon)\lambda+(\gamma_0+\gamma_1\epsilon+\gamma_2\epsilon^2)=0 \qquad (15)$$

where α_0, β_0, and γ_0 are the same as those defined in Eq. (12), but α_1, β_1, γ_1, γ_2, and ϵ are changed to

$$\alpha_1 = 4\pi\xi(S_{pq}\omega_{pq}+S_{mn}\omega_{mn})$$

$$\beta_1 = -4\pi\xi i[S_{mn}\omega_{mn}(\omega_{mn}+2\omega_{pq})+S_{pq}\omega_{pq}(\omega_{pq}+2\omega_{mn})]$$

$$\gamma_1 = -2\omega_{mn}\omega_{pq}\alpha_1$$

$$\gamma_2 = (\omega_{mn}-\omega_{pq})^2 R_{mn}^2(\xi)R_{pq}^2(\xi)\xi^2$$

$$\epsilon = \frac{k_z}{\rho h\xi}.$$

The square root branch points of the function $\lambda(\epsilon)$ are the roots of a cubic equation

$$-4\gamma_2\alpha_1\epsilon^3+(\beta_1^2-4\gamma_1\alpha_1-4\gamma_2\alpha_0)\epsilon^2 + 2(\beta_0\beta_1-2\gamma_0\alpha_1-2\gamma_1\alpha_0)\epsilon+\beta_0^2-4\alpha_0\gamma_0=0 \qquad (16)$$

Since in cases A, C, and D we are interested in the situations where ω_{mn} is almost equal to ω_{pq}, or $|\omega_{mn}-\omega_{pq}| \ll |\omega_{mn}|$, it follows that γ_2 is very small. For the purpose of estimating the roots of Eq. (16), which are closest to the origin, γ_2 may be neglected so that Eq. (16) is reduced to a quadratic equation. In this way the square root branch points of $\lambda(\epsilon)$ can be found at

$$\epsilon_\pm = T_\pm(\omega_{mn}-\omega_{pq})$$

where

$$T_\pm = \frac{4\pi\alpha_0\xi[2\omega_{mn}\omega_{pq}(S_{mn}-S_{pq})-(\omega_{mn}\sqrt{S_{mn}}\pm i\omega_{pq}\sqrt{S_{pq}})^2]}{[\omega_{mn}(\omega_{mn}-2\omega_{pq})S_{mn}+\omega_{pq}(\omega_{pq}-2\omega_{mn})S_{pq}]^2+8\omega_{mn}\omega_{pq}(\omega_{mn}-\omega_{pq})^2S_{mn}S_{pq}}.$$

It is noted that the second term in the denominator is very small compared to the first term because $(\omega_{mn}-\omega_{pq})^2$ is negligible. In case A, where w_{mn} is a backward wave and w_{pq} is a reflected wave, $S_{mn} > 0$ and $S_{pq} < 0$. In general, the absolute values of S_{mn} and S_{pq} differ significantly because they are determined by different modeshapes. Consequently, the bracket term in the numerator is real and positive. Now since α_0 is negative in case A, both T_+ and T_- are real and negative. When $\Omega > \Omega_d$ we have $\omega_{mn} < \omega_{pq}$ and the branch points $\epsilon_\pm$ are real and positive. When ϵ is real and in the range (ϵ_-, ϵ_+), the imaginary parts of $\lambda_\pm$ coincide and merging occurs, similar to the case of m_z with $\Omega < \Omega_d$. On the other hand, when $\Omega < \Omega_d$, $T_\pm$ are real and negative and no merging occurs. In both cases C and D, $T_\pm$ are complex conjugates and so are $\epsilon_\pm$. The analyses and conclusions are then the same as those in the case of m_z.

In the final case B, for which a backward wave $(m, n)_b$ meets its complex conjugate at the critical speed, β_0 and β_1 vanish. In this case $|\omega_{mn}-\omega_{pq}| \approx 2|\omega_{mn}|$ and γ_2 is no longer negligible. Equation (16) can then be reduced to

$$\lambda^2 = -\omega_{mn}\left[\omega_{mn}+\frac{R_{mn}^2(\xi)\xi\epsilon}{2\pi(\omega_{mn}+n\Omega)R_{mn}^*}\right]. \qquad (17)$$

For Ω higher than the critical speed, $\omega_{mn} < 0$ and $\lambda(\epsilon)$ has a positive branch point

$$\epsilon^* = \frac{-2\pi\omega_{mn}(\omega_{mn}+n\Omega)R_{mn}^*}{R_{mn}^2(\xi)\xi}$$

which corresponds to k_z^* in Fig. 7(*b*). For $\epsilon < \epsilon^*$, the bracket in Eq. (17) is negative and $\lambda_\pm$ are purely imaginary. On the other hand, for $\epsilon > \epsilon^*$, $\lambda_\pm$ are real numbers. When Ω is lower than the critical speed, ϵ^* is real and negative and $\lambda_\pm$ are always purely imaginary for $\epsilon > 0$. These analyses verify the results shown in Figs. 7(*a*) and 7(*b*).

Effects of Transverse Damping c_z

Figure 8 shows the effect of c_z = 0.01Ns/m on the eigenvalues in case A. It is noted that the imaginary parts of the degenerate eigenvalues for modes $(0,1)_b$ and $(0,2)_f$ at Ω_d remain degenerate, while their real parts separate with one remaining zero and the other decreasing. No merging occurs in either the real or imaginary parts. Similarly, for cases B, C, and D we observe that the imaginary parts of the degenerate eigenvalues remain degenerate and unchanged, while the real parts separate with one remaining zero, and the other decreasing, increasing, or remaining unchanged, for cases C, D, and B, respectively. Again, it is verified through additional calculations that a two-mode approximation is satisfactory in the case of c_z.

Based on the two-mode approximation, it is found that for $\Omega = \Omega_d$ and $\omega_{mn} = \omega_{pq} = \omega$, the perturbed eigenvalues are $i\omega$ and $-\frac{\beta_1}{\alpha_0}\epsilon + i\omega$, where α_0 is defined in Eq. (12) and β_1 is changed to

$$\beta_1 = 4\pi\omega_{mn}\omega_{pq}\xi(S_{mn}\omega_{pq}+S_{pq}\omega_{mn}).$$

It is obvious that the imaginary parts of the eigenvalues remain unchanged at $i\omega$, one of the real parts vanishes and the other real part changes to $-\frac{\beta_1}{\alpha_0}\epsilon$. In case A, α_0 is negative and β_1 can be negative or positive, depending on the absolute values of S_{mn} and S_{pq}. Consequently, the other real part may decrease or increase, depending on the mode shapes of modes (m, n) and (p, q). In case C, both α_0 and β_1 are positive and the other real part becomes negative. In case D, $\alpha_0 > 0$ and $\beta_1 < 0$ and the other real part becomes positive. In case B, β_1 vanishes and both real parts remain zero. These analyses agree with our numerical observations.

Effects of Pitching Parameters

Numerical results show that the effects of pitching parameters are almost the same as their transverse counterparts, except that there is no interaction between two modes when one of them has no nodal diameter, i.e., $n = 0$. This is not a surprise if we examine the two-mode approximation. It can be shown easily that the procedure we have gone through for the transverse parameters applies almost in the same manner for the pitching parameters, except that we now replace $R_{mn}(\xi)$ and $R_{pq}(\xi)$ by $nR_{mn}(\xi)$ and $qR_{pq}(\xi)$, respectively. Moreover, when one of the two modes has no nodal diameter, the off-

Downloaded 16 Oct 2008 to 140.112.113.225. Redistribution subject to ASME license or copyright; see http://www.asme.org/terms/Terms_Use.cfm

diagonal terms of $\mathbf{H}_2$ in Eq. (10) vanish and no modal interaction is induced.

Effects of Friction Force F_θ

Figure 9 shows the effects of $F_\theta = 0.004$N on the eigenvalues in case A. It is noted that the imaginary parts of the degenerate eigenvalues for modes $(0,1)_b$ and $(0,2)_f$ at Ω_d remain degenerate and unchanged, while their real parts separate with one remaining zero and the other decreasing. No merging occurs in either the real or imaginary parts. Similarly, as long as F_θ is small enough, we observe the same phenomena for cases C and D. In case B, however, friction force exhibits some unique effects on the behavior of eigenvalue changes. Figure 10(*a*) shows that for $F_\theta = 0.004$N, there exists a range of rotation speed immediately around the critical speed $\Omega_c = 849.1$ rpm, in which the natural frequency loci of modes (0,5) and $(\overline{0,5})$ merge and remain zero, while the real parts separate. When $\Omega = \Omega_c$, one of the real parts remains zero and the other becomes negative. In Fig. 10(*b*) the rotation speed is fixed at 850 rpm and F_θ has the range 0 to 0.01N. The dashed lines, which are the finite element solutions, show that the natural frequency loci start to merge as F_θ increases to F_θ^* and remain so as F_θ continues increasing. The real parts coincide and remain negative for $F_\theta < F_\theta^*$, but separate for $F_\theta > F_\theta^*$. As F_θ increases to a very large value, it is found that the upper branch of the real part loci approaches zero. When we try to use eigenfunction expansion to reproduce the dashed lines by choosing the eigenfunctions with the smallest eigenvalues, we observe that the approximation deteriorates as the number of modes used in the expansion increases, as shown by the solid lines in Fig. 10(*b*). However, if we choose only the four modes $(0,5)_r$, $(\overline{0,5})_r$, $(0.5)_f$, and $(\overline{0,5})_f$ in the expansion, the result of this four-mode approximation agrees very well with the dashed lines, although the natural frequency of $(0,5)_f$, 110.7 Hz, is very large compared to the frequency range of our current interest. This phenomenon is also observed in cases A, C, and D. Consequently, a two-mode approximation can no longer exhibit all the important features of the eigenvalue changes in the case of friction force, but a properly chosen four-mode approximation is very good.

Conclusions

Modal interactions in a spinning disk-stationary load system are studied by use of a numerical finite element method and by an eigenfunction expansion method. Their mathematical structures are analyzed in detail by considering a two-mode approximation. The results can be summarized as follows:

(1) In the cases of A, C, and D, as shown in Fig. 2, for a transverse mass m_z there are two branch points $\epsilon_\pm$ associated with the eigenvalues as functions of $\epsilon = \dfrac{m_z}{\rho h \xi}$ on the complex ϵ-plane. In case A, $\epsilon_\pm$ are real and positive when $\Omega < \Omega_d$. Frequency merging occurs and instability is induced when ϵ lies between ϵ_+ and ϵ_- along the real line. If $\Omega > \Omega_d$, $\epsilon_\pm$ are real and negative and no merging occurs. In cases C and D, $\epsilon_\pm$ are complex conjugate pairs, no merging occurs but there is frequency veering.

(2) In the case of a transverse stiffness k_z, there also exist two branch points $\epsilon_\pm$ for cases A, C and D. In case A, $\epsilon_\pm$ are real and positive when $\Omega > \Omega_d$, but negative for $\Omega < \Omega_d$, just opposite to the effect of m_z. In cases C and D, $\epsilon_\pm$ are complex conjugate pairs. In case B, there exists a single real branch point ϵ^*. For Ω higher than the critical speed and $\epsilon > \epsilon^*$, merging occurs and instability is induced.

(3) In all the cases of A, B, C, and D, for a transverse damping c_z the imaginary parts of the degenerate eigenvalues remain degenerate and unchanged, while the real parts separate with one remaining zero and the other changing, except for case B, in which both real parts remain zero. No merging occurs in either the real or imaginary parts of the eigenvalues.

(4) The effects of the pitching parameters are almost the same as their transverse counterparts, except that there is no modal interaction if one of the modes has no nodal diameter.

(5) In cases A, C, and D, for friction force F_θ the imaginary parts of the degenerate eigenvalues remain degenerate and unchanged, while the real parts separate with one remaining zero and the other changing. No merging occurs in either the real or imaginary parts of the eigenvalues. In case B, however, there exists a range of rotation speeds immediately around the critical speed in which the natural frequency loci merge and remain zero, while the real parts separate. Unlike the transverse and pitching parameters, at least four modes are required in the eigenfunction expansion to reproduce the characteristics of the eigenvalue changes due to friction force.

Acknowledgment

This work was supported by the Computer Mechanics Laboratory at the University of California at Berkeley.

References

Bender, C. M., and Orszag, S. A., 1978, *Advanced Mathematical Methods for Scientists and Engineers*, McGraw-Hill, New York.

Chen, J.-S., and Bogy, D. B., 1991, "Effects of Load Parameters on the Natural Frequencies and Stability of a Flexible Spinning Disk with a Stationary Load System," ASME JOURNAL OF APPLIED MECHANICS, to appear.

Courant, R., Hilbert, D., 1962, *Methods of Mathematical Physics*, John Wiley and Sons, New York.

Iwan, W. D., and Moeller, T. L., 1976, "The Stability of a Spinning Elastic Disk With a Transverse Load System," ASME JOURNAL OF APPLIED MECHANICS, Vol. 43, pp. 485–490.

Ono, K., Chen, J.-S., and Bogy, D. B., 1991, "Stability Analysis of the Head-Disk Interface in a Flexible Disk Drive," ASME JOURNAL OF APPLIED MECHANICS, Vol. 58, pp. 1005–1014.

Perkins, N. C., and Mote, C. D., Jr., 1986, "Comments on Curve Veering in Eigenvalue Problems," *Journal of Sound and Vibration*, Vol. 106, No. 3, pp. 451–463.

Stakgold, Ivar, 1979, *Green's Functions and Boundary Value Problems*, John Wiley and Sons, New York.

Downloaded 16 Oct 2008 to 140.112.113.225. Redistribution subject to ASME license or copyright; see http://www.asme.org/terms/Terms_Use.cfm